Electrochemical preparation of aluminium-nickel alloys by Under-Potential Deposition in molten fluorides

M. Gibilaro, L. Massot *, P. Chamelot, P. Taxil

Laboratoire de Génie Chimique UMR 5503, Département Procédés Electrochimiques
Université Paul Sabatier, 31062 Toulouse Cedex 9, France

(*) : corresponding author
Massot Laurent
Tel : +33 561558194
Fax : +33 561556139
massot@chimie.ups-tlse.fr

Abstract:

The electrochemical behaviour of AlF_3 was investigated in LiF-CaF_2 medium first with inert tungsten and then with reactive nickel electrodes. Cyclic voltammetry, square wave voltammetry and chronopotentiometry indicated that the reduction of Al(III) in Al(0) is a single-step process exchanging 3 electrons:

$Al(III) + 3e^- = Al$

The electrochemical reduction is controlled by the diffusion of AlF_3 in the solution. On a nickel electrode, a depolarisation effect for Al(III) reduction was observed in cyclic voltammetry due to the formation of Al-Ni alloys when aluminium ions react with the nickel substrate. Galvanostatic and potentiostatic electrolyses on a nickel electrode led to the formation of four nickel aluminides characterised by SEM: $AlNi_3$, AlNi, Al_3Ni_2 and Al_3Ni. Layers with a uniform composition of $AlNi_3$, AlNi and Al_3Ni_2 were prepared by varying the electrolysis potential, the current density and duration of intermetallic diffusion.

Keywords: molten fluorides; aluminium; reactive electrode; aluminides; Under-Potential Deposition.

1. Introduction

Intermetallic aluminides of transition metals such as nickel exhibit advantageous properties: high tensile strength, low density and corrosion resistance at high temperature [1,2]. Therefore these materials were investigated for their possible use as high-temperature structural materials. Moreover, transition metal aluminides have

sufficient aluminium content to form an adherent alumina layer on the surface when exposed to air or oxygen atmospheres [3] leading to excellent oxidation resistance in these intermetallic compounds.

Such alloys can be prepared in various ways and anyway the method used depends on the product desired.

Ways for obtaining aluminium nickel alloys include:

- melting both elements (the most conventional way) in an induction furnace at about 1600°C under argon atmosphere [4,5].
- using the mechanical alloying process (solid state reaction) for the production of nanocrystalline Al-Ni compounds at P = 7.7 GPa and T = 1000 °C [6].
- annealing of infiltrated aluminium-nickel precursors where nickel and molten aluminium were heat-treated at 1200 °C under argon atmosphere [7].

In this article, a novel method for nickel aluminide production was investigated using electrodeposition in molten fluoride media reacting the aluminium deposited and the nickel substrate. Our laboratory has a large experience in this field [8-10]. The electrochemical operating conditions in fluoride salts are less drastic than the techniques cited above: (1) temperature between 800 and 900°C; (2) argon atmosphere at about 1 bar. Besides, the following advantages make the process relevant:

- the composition of the alloy can be controlled by the electrolysis parameters;
- due to the reaction being controlled by intermetallic diffusion rather than transfer from the electrolyte, the shape of the substrate should not influence the uniformity of the alloy layer.

Thus, the process proposed in this article consists of aluminium electrodeposition on a reactive nickel cathode in the LiF-CaF_2 eutectic to yield Al-Ni alloys on the electrode surface.

Determining the electrochemical behaviour of Al(III) in molten salts on each type of cathodic substrate is a prerequisite for understanding how to obtain either the pure metal or compounds of the binary phase diagram.

The literature reports aluminium deposition results in molten chloride media, only on an inert cathode: Mohamedi et *al.* [11], Chryssoulakis et *al.* [12], Bouteillon et *al.* [13] agree that $AlCl_3$ is reduced to Al metal in chloride media in a single step with three electrons exchanged. Similar behaviour is reported by other authors in chloroaluminate baths [14,15].

Nevertheless, Al(III) electroreduction in fluoride media both on inert and reactive cathodes is absent from the literature. So, this article will attempt to provide data on this system for the selective preparation of Al or Al-Ni compounds in molten fluorides. It will be structured in two parts: in the first part, we studied the electroreduction of Al(III) ions on an inert W electrode by electrochemical techniques: cyclic voltammetry, square wave voltammetry and chronopotentiometry techniques. The second part reports the formation of nickel aluminides by electrodeposition of Al(III) ions on a reactive electrode (nickel) over a potential range that is less cathodic than that enabling the deposition of pure aluminium metal (Under-Potential Deposition, UPD).

2. Experimental

The cell consisted of a vitreous carbon crucible placed in a cylindrical vessel made of refractory steel and closed by a stainless steel lid cooled inside by circulating water. The inner part of the walls was protected against fluoride vapours by a graphite liner containing the experimental crucible. The experiments were performed under an inert argon atmosphere (U-grade: less than 5 ppm O_2), previously dehydrated and deoxygenated using a purification cartridge (Air Liquide). The cell was heated using a programmable furnace and the temperature was measured using a chromel-alumel thermocouple. A more detailed description of the device can be found in previous papers from our laboratory such as the one referred in [16].

The electrolytic bath consisted of the eutectic LiF/CaF_2 (SDS 99.99%) mixture (81/19 molar ratio). Before use, it was dehydrated by heating under vacuum (3.10^{-2} bar) from the room temperature up to its melting point (762 °C) for 72 h. To provide aluminium ions, aluminium fluoride AlF_3 powder (SDS 99.95%) was introduced into the bath through a chamber under argon gas atmosphere.

Electrodes: tungsten and nickel wires (1 mm diameter) were used as working electrodes. The surface area of the working electrode was determined by measuring its immersion depth in the bath after withdrawal from the cell. The auxiliary electrode was a vitreous carbon rod (3 mm diameter) with a large surface area.

All potentials are referred to a platinum wire (0.5 mm diameter) immersed in the molten electrolyte, acting as a quasi-reference electrode $Pt/PtO_x/O^{2-}$ [17].

- Electrochemical equipment: all electrochemical studies and electrolyses were performed with an Autolab PGSTAT 30 potentiostat/galvanostat controlled by a computer using the research software GPES 4.9.

- Electrochemical techniques: cyclic voltammetry, square wave voltammetry and chronopotentiometry were used for the investigation of the aluminium reduction process.
- Characterisation of reduction products: after electrolysis runs, the cathode surface was examined with a scanning electron microscope (LEO 435 VP) equipped with an EDS probe (Oxford INCA 200).

3. Results and discussion

3-1 Study of aluminium reduction on an inert electrode

At the experimental temperature of 860 °C, aluminium can form alloys or intermetallic compounds with several of the metals, except tungsten, often used as working electrodes. The present study therefore used a tungsten working electrode.

3-1-1 Cyclic voltammetry

A series of cyclic voltammetry experiments were carried out on a tungsten electrode. On the cyclic voltammogram of LiF-CaF_2-AlF_3 ($C_0 = 1.82\ 10^{-4}$ mol.cm^{-3}) presented in Fig. 1, plotted at 860 °C and 100 mV.s^{-1}, a single peak is observed in the cathodic run at around 1.25 V vs. Pt. This peak is associated with an oxidation peak at around -1 V vs. Pt. The quasi-reversibility of the system involved in this peak couple can be noted.
The cathodic peak intensity increased linearly with the concentration of aluminium (III) ions (Fig. 2), confirming that the peak can be attributed to the Al(III) reduction reaction.

Moreover, the reoxidation peak shape is typical of the dissolution of a metal deposited during a cathodic run (stripping peak).

In order to get more information on the system, the influence of the scan rate on the peak intensity was studied (Fig. 3) to verify the Berzins Delahaye relationship, valid for a reversible soluble/insoluble system and a diffusion-controlled reaction [18]:

$$I_p = -0.61nFSC_0\left(\frac{nF}{RT}\right)^{1/2} D^{1/2}\upsilon^{1/2} \quad (1)$$

where n is the number of electrons exchanged, F the Faraday constant (96500 C), S the electrode surface area in cm², D the diffusion coefficient in $cm^2.s^{-1}$, C_0 the solute concentration in $mol.cm^{-3}$, T the absolute temperature in K and υ the potential scanning rate in $V.s^{-1}$.

The linear relationship observed in Fig. 3 between ip and $v^{1/2}$ confirms the above assumptions:

- the reaction yields an insoluble product, likely aluminium metal
- the electrode process is diffusion controlled

The slope of this linear equation is found to be:

$$\frac{i_p}{v^{1/2}} = -0.4228 \pm 0.002\ A.s^{1/2}.V^{-1/2}.cm^{-2} \quad (2)$$

at T = 860 °C and $C_0 = 1.82\ 10^{-4}$ $mol.cm^{-3}$.

This result will be exploited below.

3-1-2 Chronopotentiometry

Chronopotentiometry was carried out on a tungsten electrode at 860 °C in order to further confirm the control of the electrochemical reduction process by Al(III)

diffusion. In Fig. 4, chronopotentiograms plotted at various intensities exhibit a single plateau at about -1.25 V vs. Pt corresponding to the potential for the reduction of Al(III) to Al metal, previously observed in Fig.1. The transition time τ decreased when the applied current increased and, according to Sand's law [19] valid for diffusion controlled reactions:

$$\frac{i\tau^{1/2}}{C_0} = 0.5n\pi^{0.5}FD^{0.5} \quad (3)$$

where τ is the transition time in s, n is the number of electrons exchanged, F the Faraday constant (96500 C), D the diffusion coefficient in $cm^2.s^{-1}$ and C_0 the solute concentration in $mol.cm^{-3}$.

The data plotted in Fig. 5 are not influenced by C_0, which is in accordance with the Sand equation mentioned above; the validity of this reaction was confirmed at other temperatures.

At 860 °C, the value of C_0 is given by:

$$\frac{i\tau^{1/2}}{C_0} = -605.13 \pm 0.2 \text{ A.cm.s}^{1/2}.\text{mol}^{-1} \quad (4)$$

Likewise this result will be used below.

The reversal chronopotentiogram presented in Fig.6 ($C_0 = 1.99\ 10^{-4}$ $mol.cm^{-3}$ and $I = -70$ $mA.cm^{-2}$) exhibits an anodic transition time equal to the cathodic one ($\tau_{ox} = \tau_{red} = 2.9$ s). This result, typical of the formation of an insoluble compound on the electrode, seems to confirm, once again, the formation of Al metal on the cathode.

3-1-3 Number of electrons exchanged

The final proof of the formation of Al by reduction of Al(III) in one step at -1.25 V vs. Pt was provided by the calculation of the number of electrons exchanged.

Two different methods were used for the calculation:

- combination of cyclic voltammetry and chronopotentiometry measurements
- square wave voltammetry

- The first method gives the following relationship, after coupling (1) and (3), and allows the uncertainty on the Al(III) concentration and diffusion coefficient to be ignored:

$$\frac{I_p / \sqrt{\upsilon}}{I\sqrt{\tau}} = 74.173\sqrt{\frac{n}{T}} \qquad (5)$$

In the example of equations (1) and (3), the calculated number of electrons exchanged was found to be 3.1 ± 0.1. It can be concluded that 3 electrons are exchanged by the aluminium (III) reduction, according to the reaction:

$$Al(III) + 3e^- = Al \qquad (6)$$

- The other technique used to determine the number of electrons exchanged was square wave voltammetry [20]. In this method, derived from cyclic voltammetry, the scanning of potential proceeds stepwise with superimposition, on each step of the staircase, of two potential pulses, direct and reverse, with equal values. Plotting the differential intensity measured at each step between the successive pulses versus the potential associated to each electrochemical reaction provides a Gaussian shaped peak . In the case of a reversible system, mathematical analysis of the peak yields a simple equation associating the half-width of the peak ($W_{1/2}$) and the number of electrons exchanged:

$$W_{1/2} = 3.52 \frac{RT}{nF} \quad (7)$$

A typical square wave voltammogram of the system $LiF\text{-}CaF_2\text{-}AlF_3$ ($C_0 = 1.82\ 10^{-4}$ mol. cm^{-3}) is shown in Fig. 7 at T = 860 °C and f = 9 Hz. The curve exhibits one peak at about -1.2 V/Pt corresponding to the $E_{p/2}$ of the cyclic voltammogram. Beforehand, we verified the validity of Eq. (7) in Fig. 8, as far as the frequency of the signal has to be in a linearity range of the current peak with the square root of the frequency [21,22]. The choice of the lowest frequency in the range is justified by the greater sensitivity of the method at low frequency.

Measuring $W_{1/2}$ ($W_{1/2}$: 112mV in this figure) gives an average value for the number of electrons exchanged of 3.06 ± 0.1. So, this result confirms that Al(III)/Al(0) reduction proceeds in a single step.

The determination of the peak potential by the square-wave voltammogram in Fig.7 gives the half wave potential of Al(III) reduction. This value was found to be 1.20 ± 0.01 V vs. Pt.

3-2 Nickel aluminide alloy formation

The characteristics of pure aluminium electrodeposition having been determined, in particular its potential range, we will now examine the electrodeposition of aluminium compounds obtained by the reaction of Al(III) with a nickel cathodic material.

According to the Al-Ni phase diagram shown in Fig. 9 [23], aluminium can form various alloys with nickel: one intermetallic compound Al_3Ni and four other phases Al_3Ni_2, AlNi, Al_3Ni_5 and $AlNi_3$ for which a wide range of stoichiometric compositions is noted.

The variability of the stoichiometric proportions of certain phases of the Ni-Al alloys prevents the accurate determination the Gibbs energy of each compound of the Al-Ni binary diagram by the relaxation method, long used in our group and more recently described by Nourry *et al*. for the Nd-Ni system [24]. This method, based on the measurement during intermetallic diffusion of potential plateaus associated to the coexistence of two phases with a well defined composition at the substrate surface, is not accurate if the composition of the surface compound varies.

The method fails for the Al-Ni system because the potential plateaus are not well enough defined, due to the composition variation of of the compounds coexisting at each plateau. Nevertheless, part of these thermodynamic data are available in the bibliography [25, 26]. According to these references, the most stable alloys are Al_3Ni_2, then Al_3Ni and AlNi. These results were confirmed with the calculation of the Gibbs energy thanks to the SGTE database [27].

As in previous articles by our team for other systems – for instance Nd-Ni [24], Sm-Ni [28] and Ta-Ni [29] – Al(III) must be reduced to Al-Ni compounds under the deposition potential of the pure metal (UPD). The depolarisation of Al(III) discharge is due to the Gibbs energy of the compound. The identification and the characterisation of these compounds were performed by cyclic voltammetry and SEM analysis.

3-2-1 Cyclic voltammetry

A cyclic voltammogram of the electrodeposition of aluminium on a nickel cathode at T = 860 °C with a scan rate of 100 $mV.s^{-1}$ is compared in Fig. 10 to the one drawn with an inert electrode. On the reactive electrode, one reduction wave is observed at -0.85 V

vs. Pt prior to the peak of the pure Al deposition observed on a tungsten electrode at -1.25 V vs. Pt. This additional current observed at UPD is attributed to the formation of Al-Ni alloys. This confirms that Al(III) reduction is depolarised by the formation of Al-Ni alloys and shows that alloys can be yielded by electrolysis in the potential range from -0.9 up to -1.25 V vs. Pt.

3-2-2 Electrolysis runs

In order to examine the results of the reduction of Al(III) at UPD on nickel, galvanostatic and potentiostatic electrolyses were performed at [Al(III)] = 3.57 10^{-4} mol.cm^{-3} and the electrolysis parameters (time, current density or potential) were widely varied; just after each run the alloyed electrode is quenched by rapid withdrawal from the cell.

The cross sections of samples after electrolysis are presented in Figs. 11, 14 and 15. An EDS probe allowed us to determine all the composition phases observed on micrographs.

The purpose of these experiments is to examine what compounds of the binary Al-Ni diagram it is possible to prepare and the specific conditions required to obtain them. Obviously, the alloy layer compositions result from two physical phenomena: electrochemical reduction and intermetallic diffusion; the first can be controlled; the second occurs anyway and should lead to thermodynamically stable compounds in the alloy layer.

For a complete analysis of all the possible situations, we worked under three types of electrolysis condition:

- potentiostatic electrolysis
- galvanostatic electrolysis
- galvanostatic electrolysis followed after opening the electrical circuit by keeping the cathodic sample in the molten salt for several hours.

3-2-2-a Potentiostatic electrolysis

Nickel aluminides can be prepared using potentiostatic electrolysis at various potentials (from -0.8 to 1.25 V vs. Pt). The alloy composition is determined by the potential of the electrolysis. These electrolyses were performed at 860 °C for 1200 s on nickel electrode:

- (I) E = -0.9 V vs. Pt. In the micrograph shown in Fig. 11a, one aluminium-nickel compound is observed, confirming once again that Al(III) can be reduced at UPD. This compound has the composition of $AlNi_3$ which is the alloy with the highest Ni content on the phase diagram. This result was foreseeable as far as at low cathodic potentials, the formation of the compound with the highest nickel content can only be expected. Moreover, at this potential, the electrolysis current is low and decreases according to a Cottrell type law as shown in Fig. 12, this explains that the layer is very thin (less than 10 μm) and porous.

- (II) E = -1.25V vs. Pt. At this potential pure aluminium can be deposited but it diffuses into the bulk of the cathode. So, all the compounds of the binary system can be expected. In fact, two alloys are observed on the nickel substrate (Fig. 11b): $AlNi_3$ and Al_3Ni_2. The $AlNi_3$ layer was close to the nickel boundary and was also very

thin (less than 3 μm). The major part of the layer consisted of a homogeneous, compact Al_3Ni_2 compound. We notice that: (i) the Al_3Ni phase, with the highest Al content, predicted by the Al-Ni phase diagram is missing, this confirms the stability of Al_3Ni_2 mentioned above and (ii) the yield, only at the substrate boundary, of a compound with a higher nickel content ($AlNi_3$), due to the excess nickel is observed.

3-2-2-b Galvanostatic electrolysis

The galvanostatic mode of electrolysis presents the advantage of keeping a constant, high rate of alloy layer growth. However, this mode makes it impossible to control the specific formation of a compound since, due to the saturation occurring at the cathode surface, the whole series of compounds of the system are successively formed at the cathode. Simultaneously to the electrolytic processing, the intermetallic diffusion at the cathode surface must play an important role, in theory for promoting the predominance of the most stable phase within the alloy layer.
Galvanostatic electrolysis was performed at different applied current densities, and the electrodes were quickly cooled down after aluminium deposit.

- Evolution of the cathode potential during the electrolysis

Figure 13 exhibits a typical variation of the potential during the intensiostatic electrolysis. We see in the zoom in Fig. 13 that the potential remains below the Al deposition potential (UPD) for just a short time (no more than 30 s) before levelling off at a value corresponding to that of pure Al deposition. During the UPD stage, only the

series of Al-Ni compounds are successively formed on the cathode surface; afterwards, pure Al is deposited and the rate of deposition is equilibrated by its diffusion rate within the surface alloy layer. Thus, we can expect the same result for the alloy composition as that obtained on potentiostatic electrolysis at -1.25 V vs. Pt.

- Influence of the current density on the alloy layer composition

The following runs were performed at T = 860 °C, for 3600 s and at three values of the current density:

- (I) Low current density i = -37 mA.cm^{-2}

Figure 14a shows the same phases as Fig. 13b: $AlNi_3$ at the nickel boundary and in the rest of the layer a homogeneous Al_3Ni_2 layer (thickness: 40 μm). Once again, the stability of Al_3Ni_2 is confirmed.

- (II) Increased current density i = -64 mA.cm^{-2}

In the micrograph shown in Fig. 14b, we observe that three compounds are present on the nickel surface: once again a thin layer of $AlNi_3$ at the nickel boundary, Al_3Ni_2 over most of the alloy layer (65 μm thickness) and Al_3Ni at the electrolyte interface. The presence of this compound with a high Al content at the cathode surface can be easily explained by a higher Al(III) reduction rate, yielding a greater amount of Al_3Ni to balance the excess aluminium provided by the electrolysis. So, the alloy layer on the cathode is composed of successive phases with increasing aluminium content from the nickel boundary to the electrolyte interface.

- (III) High current density i = -120 mA.cm^{-2}

The micrograph in Fig. 14c confirms the previous result since it shows the successive presence from the electrode surface to the substrate of $AlNi_3$, Al_3Ni_2 (130 μm) and Al_3Ni. Due to the higher applied current density in this experiment, the overall aluminium content of the layer is increased and promotes still more the alloys with a higher proportion of aluminium and thus an increase of the layer thickness of Al_3Ni. It can also be noted that the Al_3Ni layer melts off the cathode in the form of drops, the melting point Al_3Ni compound (T_f = 854 °C) being lower than our working temperature.

- Influence of intermetallic diffusion after electrolysis

We observed in the previous experiments that both the value of the current density and the intermetallic diffusion readily influence the composition of the alloy layer. The quenching of the electrode after the electrolysis run clearly hinders the complete extension of intermetallic diffusion. So, in further experiments, the electrode was kept in the bath after electrolysis in order to examine the influence of intermetallic diffusion of Al into the Ni and therefore on the composition of the surface alloy during this open circuit time.

The operating conditions were the following: temperature 860 °C; duration of the electrolysis run 3600 s. The variable parameters were the applied current density and the duration of contact between the cathodic sample and the melt after the electrolysis time (diffusion time).

- (I) i = -30 $mA.cm^{-2}$ and diffusion time = 2.1 hours

The result is presented in the micrograph in Fig. 15a where three compounds are observable on the nickel substrate: a thin layer of $AlNi_3$ at the nickel boundary as observed previously, due to the excess of nickel; two layers of AlNi, differing by their shade of grey on the micrograph corresponding to a difference of stoichiometry: 58 atom % Ni in the inner part 47 atom % Ni in the outer part. These values corroborate the binary diagram which report that the composition of Al-Ni can vary between 45 and 59 atom % Ni. The change during the intermetallic diffusion stage in the composition of the alloy layer from the most stable compound Al_3Ni_2 to the least stable AlNi, if we refer to [25, 26], is unexpected regarding the above forecast and appears to be the consequence of the solid reaction between Al_3Ni_2 and the nickel substrate, via compound $AlNi_3$, giving a metastable compound.

- (II) i = -42 $mAcm^{-1}$ and diffusion time = 2.8 hours

In Fig. 15b, the same composition of the surface alloy as in Fig. 15a is observed: $AlNi_3$ at the nickel boundary, AlNi (56 atomic % Ni) and AlNi (50 atomic % Ni) in the major part of the layer. This confirms that (i) the final composition of the alloy is not dependent on the electrolysis current when intermetallic diffusion proceeds for sufficient time; (ii) the theoretically stable Al_3Ni_2 is missing from the layer. Nevertheless, compared to the previous experiment, we note that the difference in nickel content in two AlNi solid phases decreases, probably due to a longer diffusion time, meaning that the diffusion time increase only yields one phase composition.

- (III) i = -70 $mA.cm^{-2}$ during 10 000 s and diffusion time = 4 hours.

The result is shown in Fig. 15c and 15d, where the composition of the surface alloy mainly consists of AlNi (48 atomic % Ni) and a thin layer of $AlNi_3$ close to the nickel boundary. This confirms that the intermetallic diffusion leads to a layer with a uniform

composition of AlNi compound, which is unexpected as it is not the most stable compound of the Al-Ni system.

4. Conclusion

In this article, the electrochemical behaviour of aluminium ions was studied in LiF-CaF_2 medium successively on an inert tungsten electrode and on a reactive nickel electrode. Applying different electrochemical techniques to investigate the system, we found that the reduction mechanism led to a one-step process exchanging 3 electrons on W: Al(III) + $3e^-$ = Al.

A depolarisation effect was observed with cyclic voltammetry when Al(III) was reduced on the nickel cathode proving that nickel aluminides are formed at UPD. The preparation of Al-Ni alloys occurred under potentiostatic and galvanostatic electrolyses and the alloy layers were characterised using SEM and EDX. Alloys with varying proportions of the two metals: Al_3Ni, Al_3Ni_2, AlNi and $AlNi_3$ were obtained under different experimental conditions. Applying a low current density, a homogeneous Al_3Ni_2 layer was obtained. However, when the nickel electrode was kept in the bath after the electrolysis time, the intermetallic diffusion changes the composition of the alloy layer to yield a homogeneous AlNi layer.

So, the conditions studied allow the preparation of three Al-Ni compounds:

- Potentiostatic electrolysis at UPD: $AlNi_3$
- Intensiostatic electrolysis: Al_3Ni_2
- Intensiostatic electrolysis, followed by a period of diffusion after opening the electrical circuit: AlNi

In conclusion, this study shows great promise for the use of the electrochemical route to prepare Al-Ni alloys exhibiting attractive properties for several fields of technology such as power generation, aerospace and anode materials for molten carbonate fuel cells.

Acknowledgements

The authors express their thanks to the PCR RSF Thorium and GDR Paris from the PACE program for financial support of this work.

References:

[1] I. Baker, P. R. Munroe, High temperature aluminides and intermetallics, Materials Research Society, Warrendale, Pennsylvannia, 1990, pp 425-457

[2] J. Brillo, A. Bytchkov, I. Egry, L. Hennet, G. Mathiak, I. Pozdnyakova, D.L. Price, D. Thiaudiere, D. Zanghi, J. Non-Cryst. Solids 352 (2006) 4008-4012

[3] S.C. Deevi, V.K. Sikka, Intermetallics 4 (1996) 357-375

[4] S.C. Deevi, V.K. Sikka, Intermetallics 5 (1997) 17-27

[5] J.E. Orth, V.K. Sikka, Advanced Materials and Processes 48 5 (1995) 33-34

[6] M. Krasnowski, A. Antolak, T. Kulik, J. Alloys Comp. 434-435 (2007) 344-347

[7] C. Dunand, J. Mater. Sci. 29 15 (1994) 4056-4060

[8] P. Taxil, P. Chamelot, L. Massot, C. Hamel, J. Min. Met. 39 1-2 B (2003) 177-200

[9] P. Taxil, Less Com. Metal. 113 1 (1985) 89-101

[10] L. Massot, P. Chamelot, P. Taxil, Electrochim. Acta 50 28 (2005) 5510-5517

[11] M. Mohamedi, N. Kawaguchi, Y. Sato, T. Yamamura J. Alloys Comp. 287 (1999) 91-97

[12] Y. Chryssoulakis, F. Lantelme, A. Alexopoulou, S. Kalogeropoulou, J. Appl. Electrochem. 18 1 (1988) 23-26

[13] J. Bouteillon, A. Marguier, Surf. Techn. 22 (1984) 205-217

[14] G. R. Stafford, G. M. Haarberg, Plasmas and Ions 1 (1999) 35-44

[15] P. Rolland, G. Mamantov, J. Electrochem. Soc. 123 9 (1976) 1299-1303

[16] P. Chamelot, P. Taxil, B. Lafage, Electrochim. Acta 39 17 (1994) 2571-2575

[17] A. D. Graves, D. Inman, Nature 208 (1965) 481-482

[18] T. Store, Thesis, Department of Electrochemistry, Norwegian University of Science and Technology, 1999

[19] R.K. Jain, H.C. Gaur, B.J. Welch, J. Electroanal. Chem. 79 (1977) 211

[20] L. Ramaley, M.S. Krause, Anal. Chem. 41 (1969) 1362

[21] P. Chamelot, P. Palau, L. Massot, A. Savall, P. Taxil, Electrochim. Acta 47 (2002) 3423-3429

[22] P. Chamelot, B. Lafage, P. Taxil, Electrochim. Acta 43 5–6 (1997) 607

[23] Binary Alloy Phase Diagrams, 2nd edition, ASM International, 1996

[24] C. Nourry, L. Massot, P. Chamelot, P. Taxil, J. New Mat. Electrochem. Systems. 10 (2007) 117-122

[25] G. Rog, G. Borchardt, M. Wellen, W. Loser, J. Chem. Thermodyn. 35 (2003) 261-268

[26] I. Barin, Thermochemical Data of Pure Substances, third ed., Chemistry, Weinheim, 1995

[27] Scientific Group Thermodata Europe http://www.sgte.org/

[28] L. Massot, P. Chamelot, P. Taxil, Electrochim. Acta 50 (2005) 5510-5517

[29] P. Taxil, J. Less-Common Met., 113 (1985) 89-101

Figure captions

Fig. 1. Typical cyclic voltammogram of the $LiF-CaF_2-AlF_3$ ($1.82\ 10^{-4}$ $mol.cm^{-3}$) system at 100 $mV.s^{-1}$ and T = 860 °C. Working electrode: W; Counter electrode: vitreous carbon; Quasi-reference electrode: Pt.

Fig. 2. Cathodic peak current density versus AlF_3 concentration.

Fig. 3. AlF_3 peak current density versus the square root of the scanning potential rate at T = 860 °C. Working electrode: W; Counter electrode: vitreous carbon; Quasi-reference electrode: Pt.

Fig. 4. Chronopotentiograms of the $LiF-CaF_2-AlF_3$ ($4.76\ 10^{-4}$ $mol.cm^{-3}$) system for different applied intensities at T = 860 °C. Working electrode: W (S = 0.44 cm^2); Counter electrode: vitreous carbon; Quasi-reference electrode: Pt.

Fig. 5. $i.\tau^{1/2} / C_0$ versus the AlF_3 concentration at 860 °C. Working electrode: W; Counter electrode: vitreous carbon; Quasi-reference electrode: Pt.

Fig. 6. Reversal chronopotentiogram of AlF_3 ($1.99\ 10^{-4}$ $mol.cm^{-3}$) in $LiF-CaF_2$, i = ± 70 $mA.cm^{-2}$ at T = 860 °C.

Fig. 7. Square wave voltammogram of LiF-CaF_2-AlF_3 (1.82 10^{-4} mol.cm^{-3}). Frequency: 9 Hz; T = 860 °C; Working electrode: W; Counter electrode: vitreous carbon; Quasi-reference electrode: Pt.

Fig. 8. Plot of the peak current density vs. the square root of the frequency. T = 860 °C; Working electrode: W; Counter electrode: vitreous carbon; Quasi-reference electrode: Pt.

Fig. 9. Aluminium Nickel phase diagram [23].

Fig. 10 Comparison of cyclic voltammograms in LiF-CaF_2-AlF_3 media on W and Ni electrodes at 100 mV.s^{-1} and T = 860 °C. Counter electrode: vitreous carbon; Quasi-reference electrode: Pt.

Fig. 11a Micrograph of the cross section of a nickel wire after electrolysis. Experimental conditions: T = 860 °C, E = -0.9 V vs. Pt, t = 3600 s.

Fig. 11b Micrograph of the cross section of a nickel wire after electrolysis. Experimental conditions: T = 860 °C, E = -1.25 V vs. Pt, t = 3600 s.

Fig. 12 Current density during potentiostatic electrolysis at E = -0.9 V vs. Pt and T = 860 °C.

Fig. 13 Nickel electrode potential during intensiostatic electrolysis versus time. Experimental conditions: T = 860 °C, i = -37 mA.cm^{-2}.

Fig. 14a Micrograph of the cross section of a nickel wire after electrolysis. Experimental conditions: T = 860 °C, i = -37 mA.cm^{-2}, t = 3600 s.

Fig. 14b Micrograph of the cross section of a nickel wire after electrolysis. Experimental conditions: T = 860 °C, i = -64 mA.cm^{-2}, t = 3600 s.

Fig. 14c Micrograph of the cross section of a nickel wire after electrolysis. Experimental conditions: T = 860 °C, i = -120 mA.cm-2, t = 3600 s.

Fig. 15a Micrograph of the cross section of a nickel wire after electrolysis. Experimental conditions: T = 860 °C, i = -30 mA.cm^{-2}, t = 3600 s and diffusion time = 2.1 h.

Fig 15b Micrograph of the cross section of a nickel wire after electrolysis. Experimental conditions: T = 860 °C, i = -42 mA.cm^{-2}, t = 3600 s and diffusion time = 2.8 h.

Fig. 15c Micrograph of the cross section of a nickel wire after electrolysis. Experimental conditions: T = 860 °C, i = -70 mA.cm^{-2}, t = 10000 s and diffusion time = 4 h.

Fig. 15d Micrograph of the cross section of a nickel wire after electrolysis.

Experimental conditions: T = 860 °C, i = -70 mA.cm^{-2}, t = 10000 s and diffusion time = 4 h.

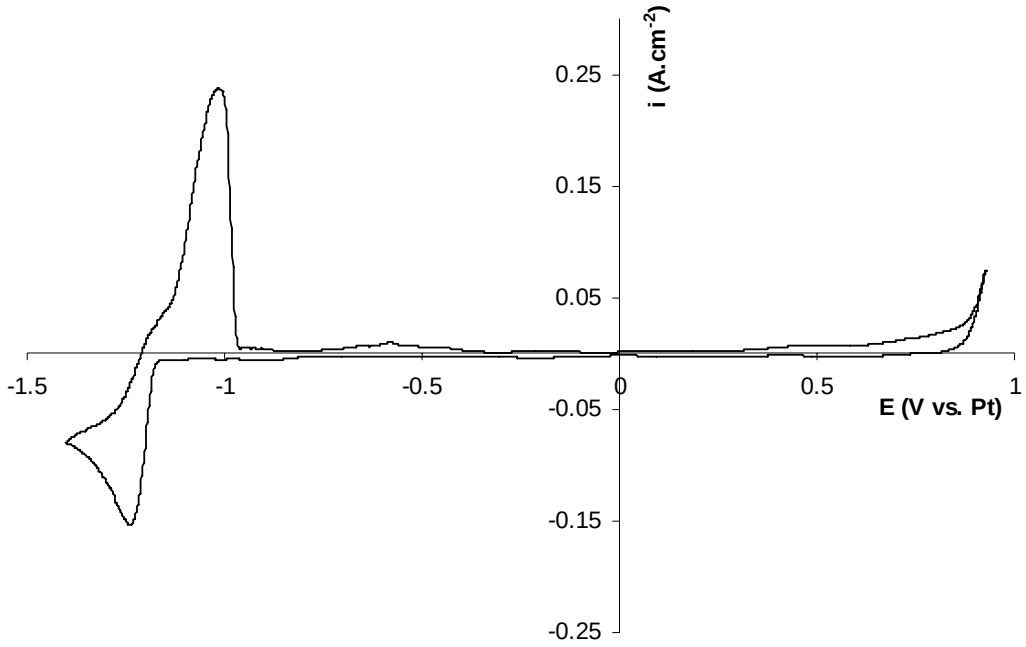

Figure 1

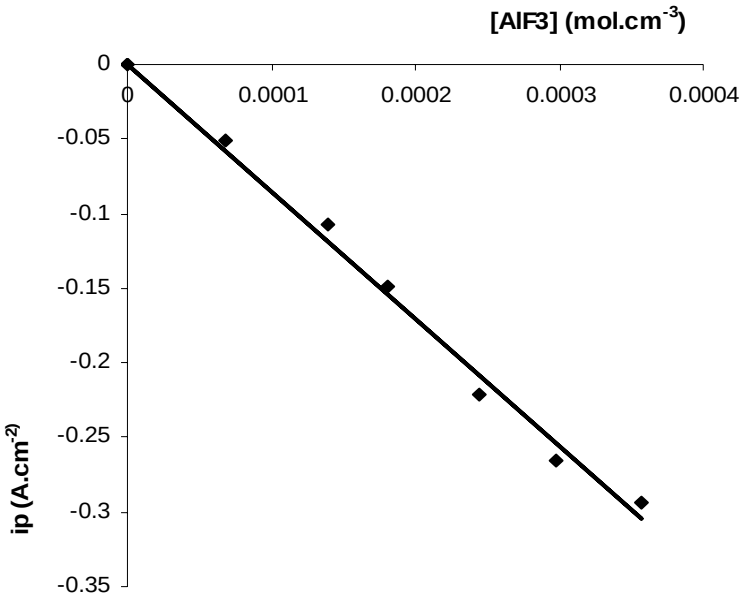
[AlF3] (mol.cm-3)
0
0
0.0001
0.0002
0.0003
0.0004
-0.05
-0.1
-0.15
-0.2
-0.25
-0.3
-0.35
ip (A.cm-2)

Figure 2

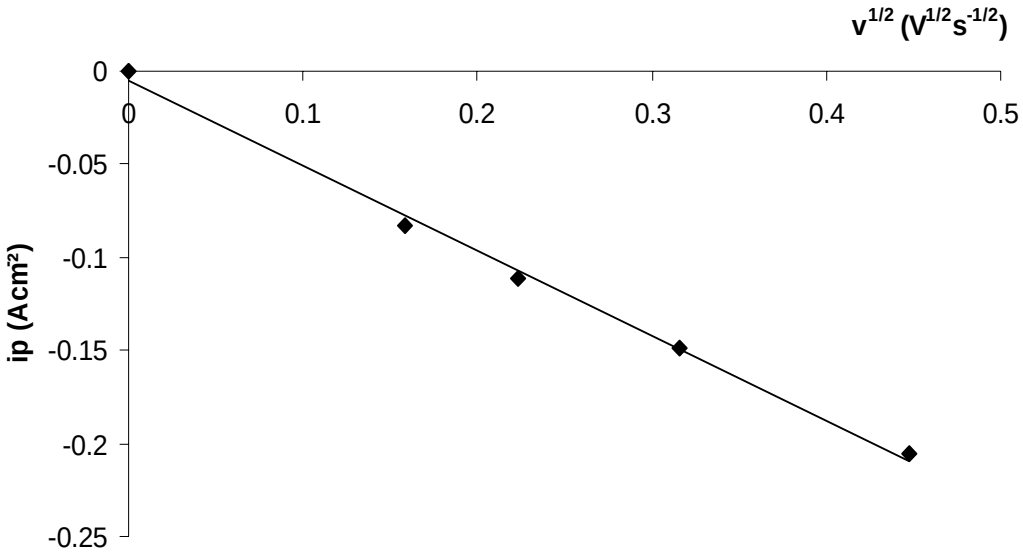

Figure 3

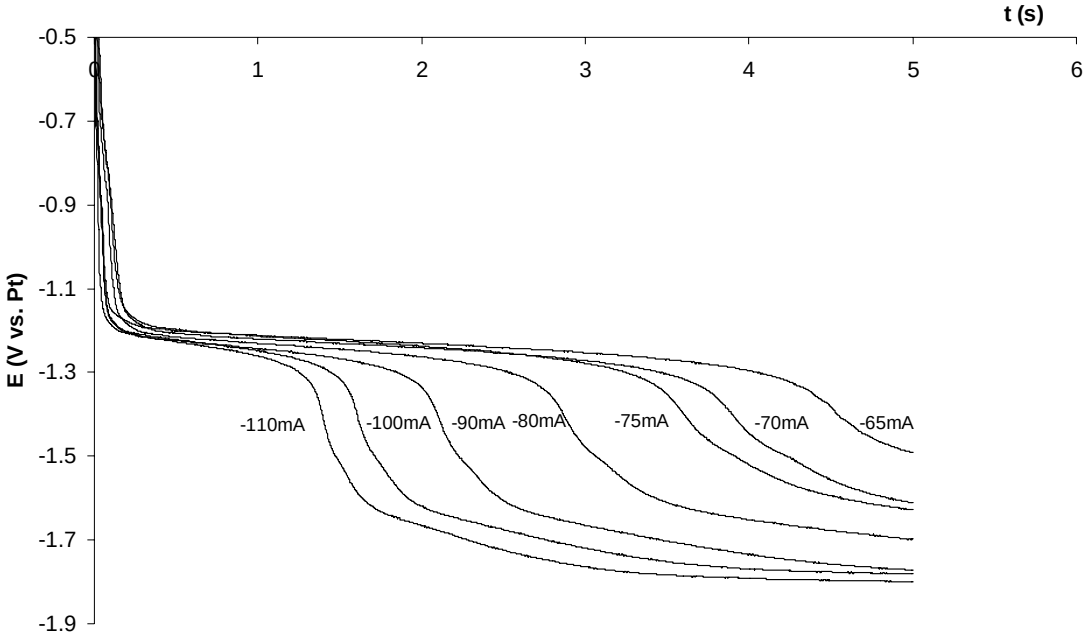
t (s)
-0.5
-0.7
-0.9
-1.1
-1.3
-1.5
-1.7
-1.9
0
1
2
3
4
5
6
E (V vs. Pt)
-110mA
-100mA
-90mA
-80mA
-75mA
-70mA
-65mA

Figure 4

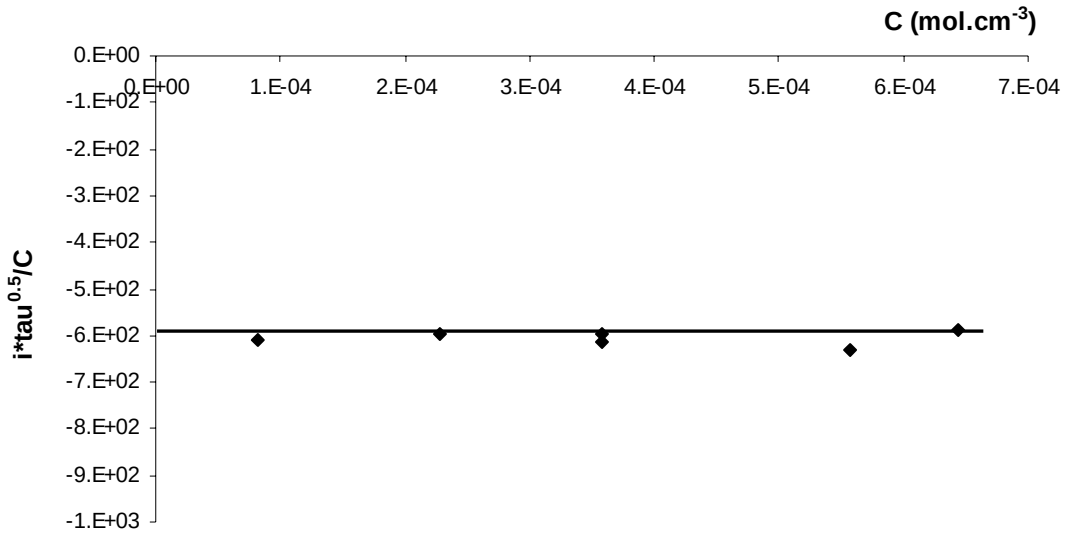
C (mol.cm-3)
0.E+00
-1.E+02
-2.E+02
-3.E+02
-4.E+02
-5.E+02
-6.E+02
-7.E+02
-8.E+02
-9.E+02
-1.E+03
0.E+00
1.E-04
2.E-04
3.E-04
4.E-04
5.E-04
6.E-04
7.E-04
i*tau0.5/C

Figure 5

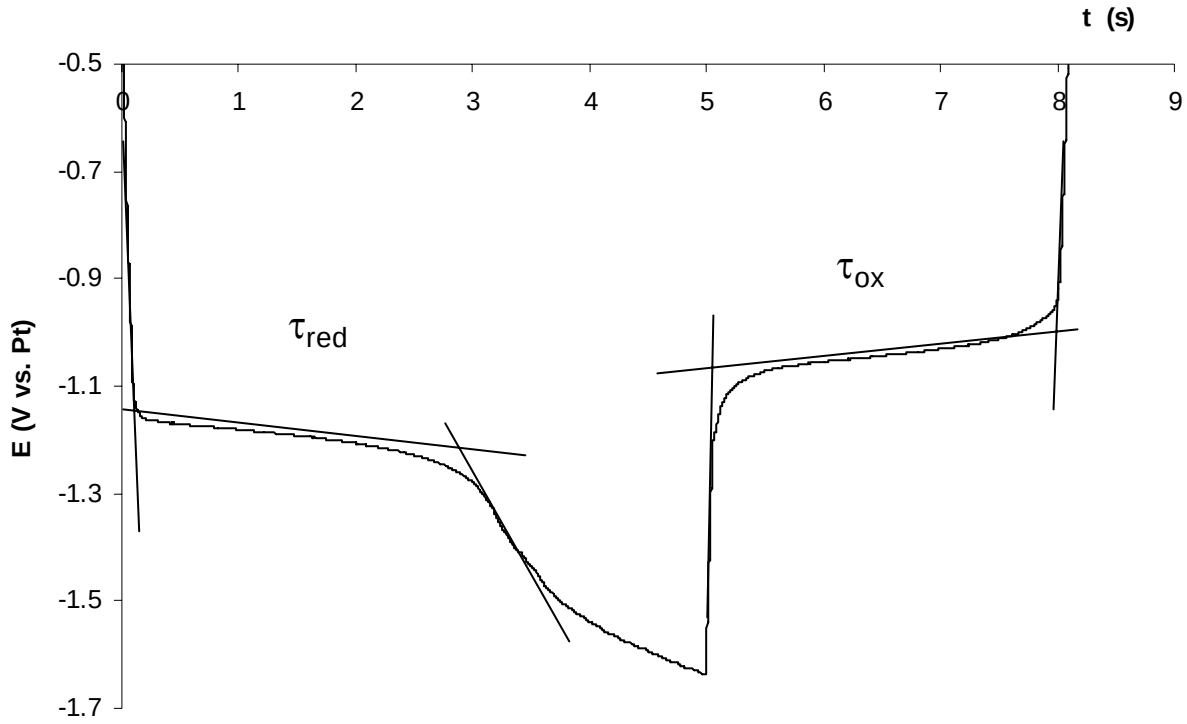

Figure 6

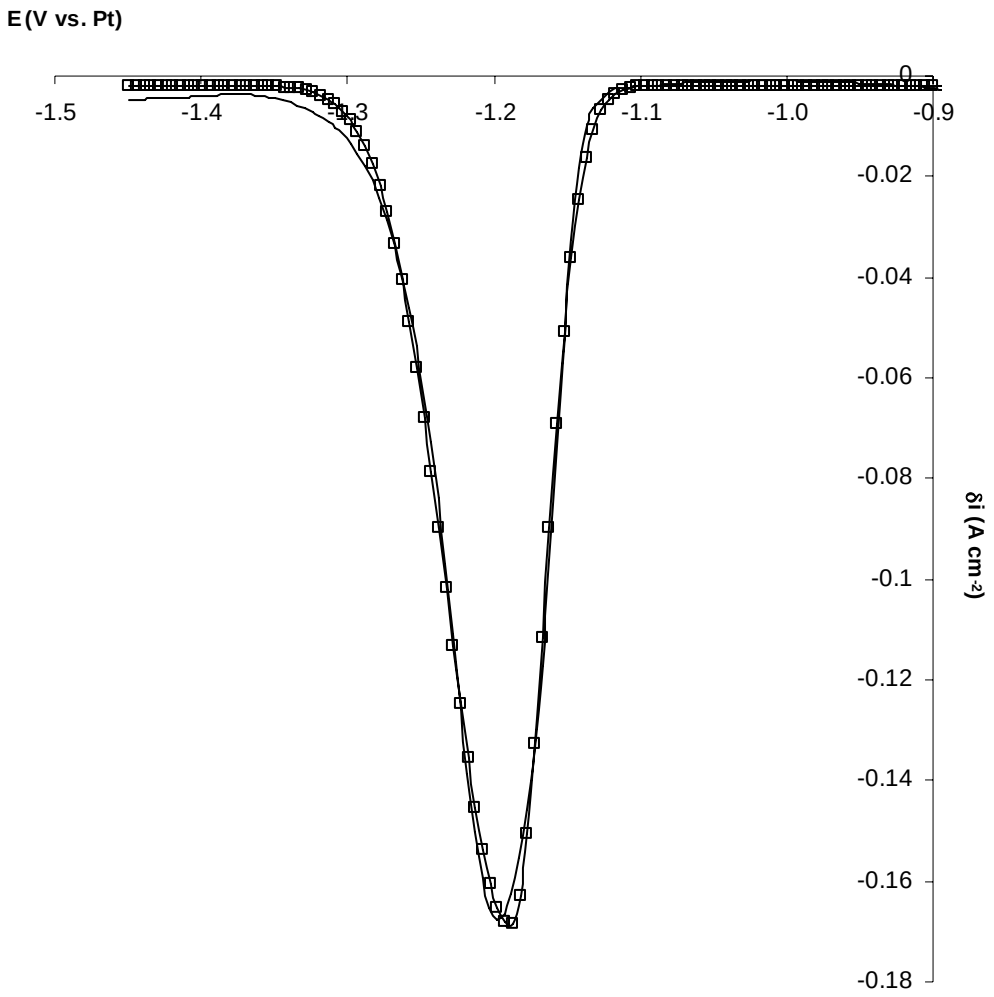
E (V vs. Pt)
0
-0.02
-0.04
-0.06
-0.08
-0.1
-0.12
-0.14
-0.16
-0.18
-1.5
-1.4
-1.3
-1.2
-1.1
-1.0
-0.9
δi (A cm-2)

Figure 7

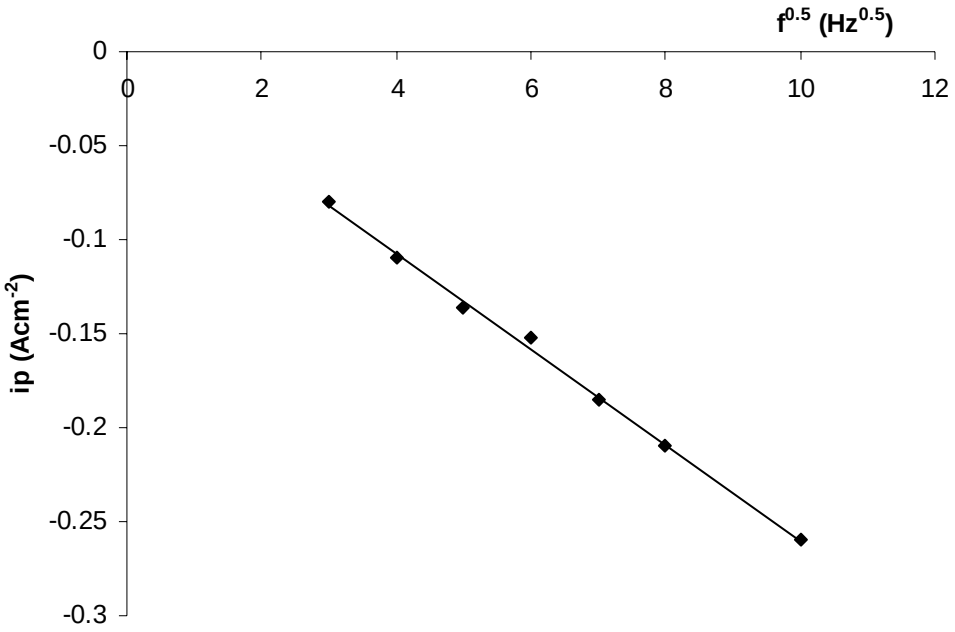

Figure 8

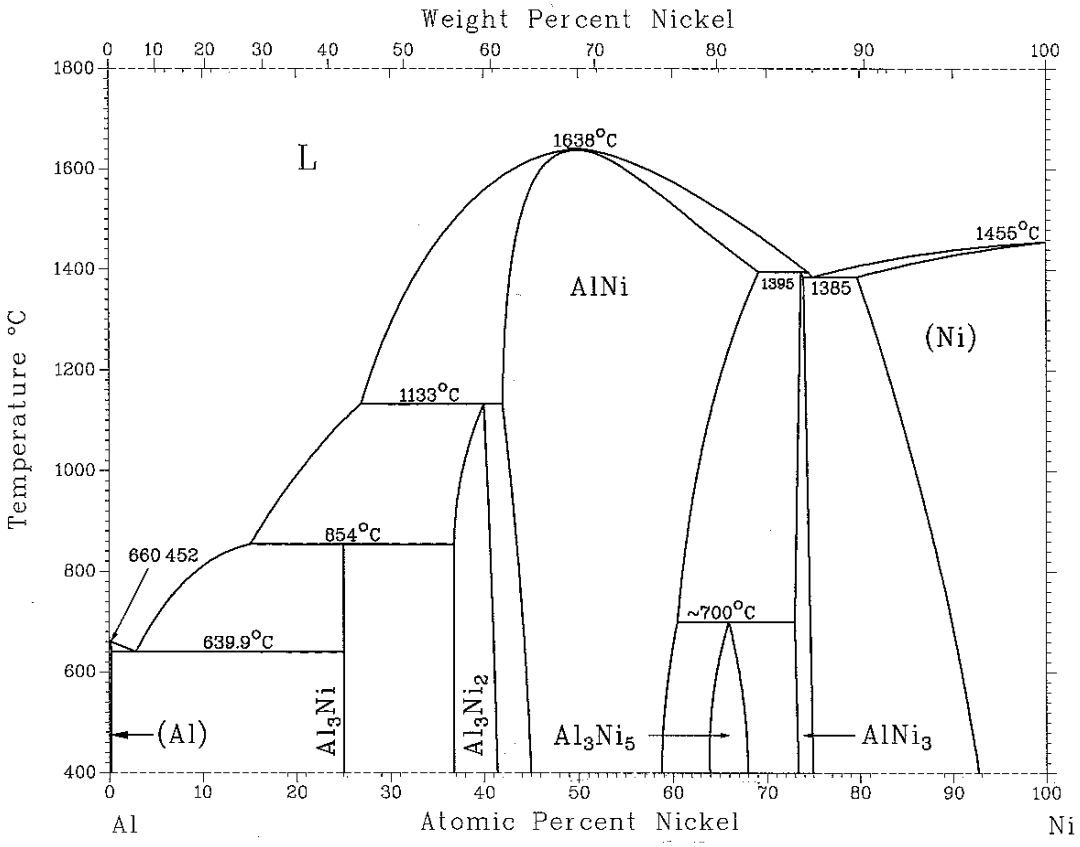
Weight Percent Nickel
0 10 20 30 40 50 60 70 80 90 100
1800
1600
1400
1200
1000
800
600
400
Temperature °C
L
1638°C
1455°C
AlNi
1395
1385
(Ni)
1133°C
854°C
660 452
639.9°C
~700°C
(Al)
Al3Ni
Al3Ni2
Al3Ni5
AlNi3
0 10 20 30 40 50 60 70 80 90 100
Al
Atomic Percent Nickel
Ni

Figure 9

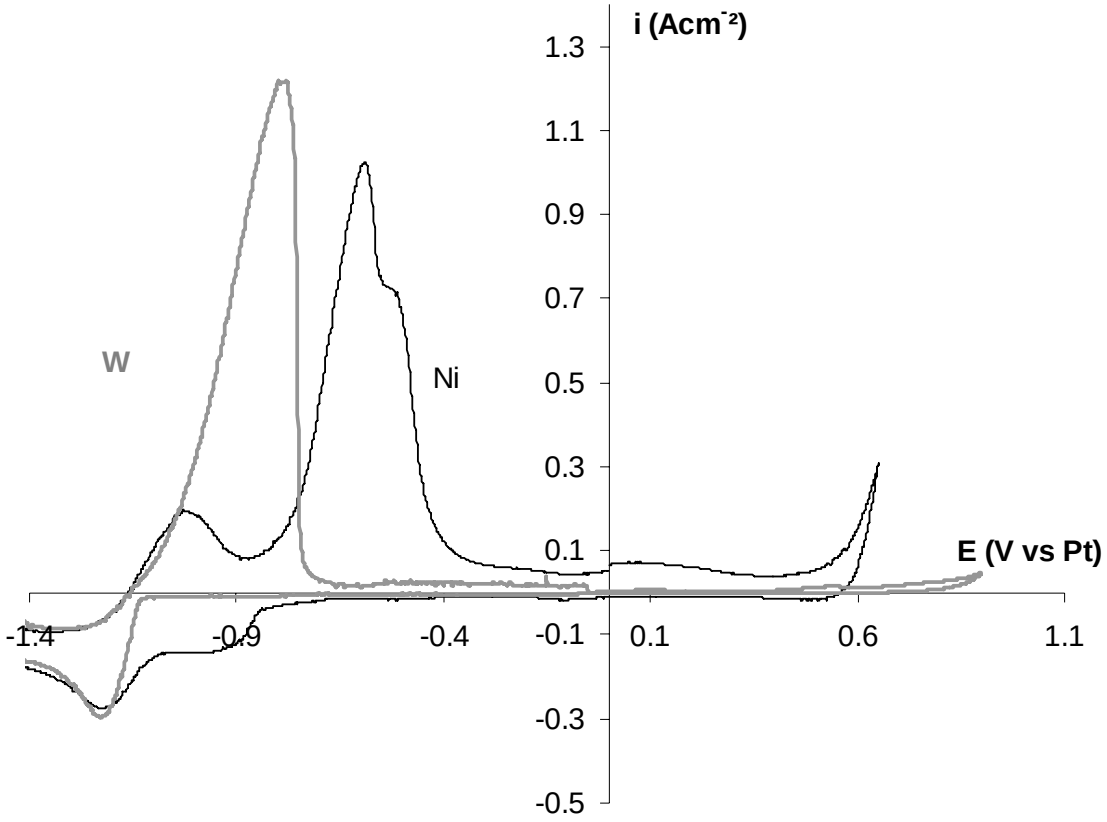

Figure 10

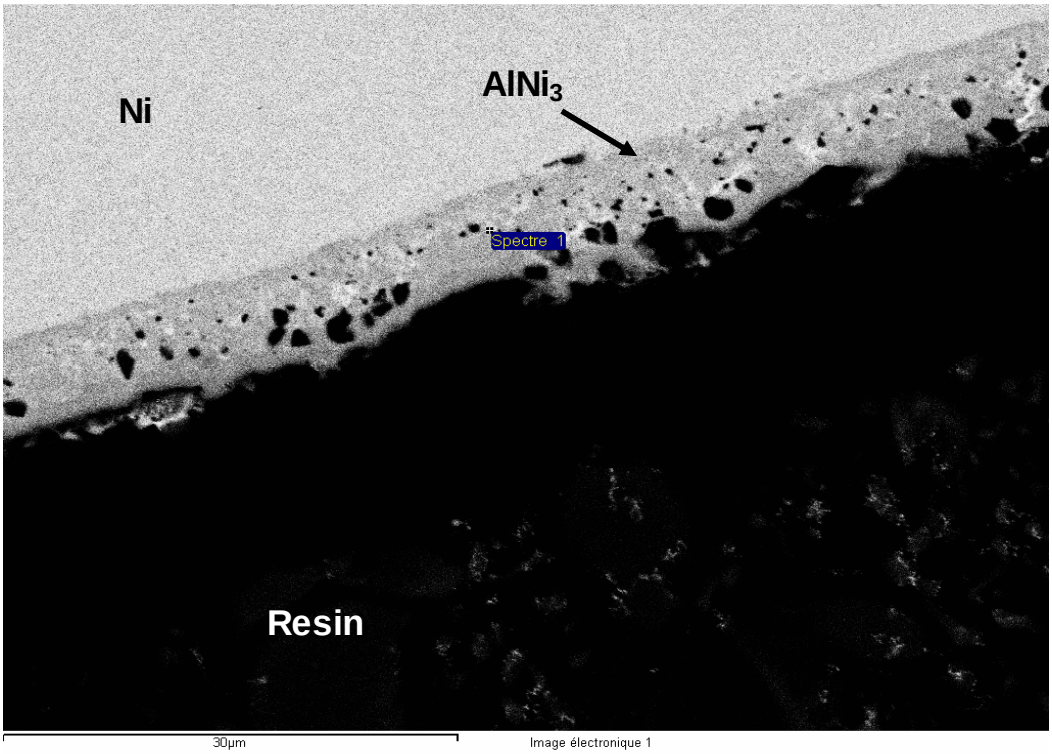

Figure 11a

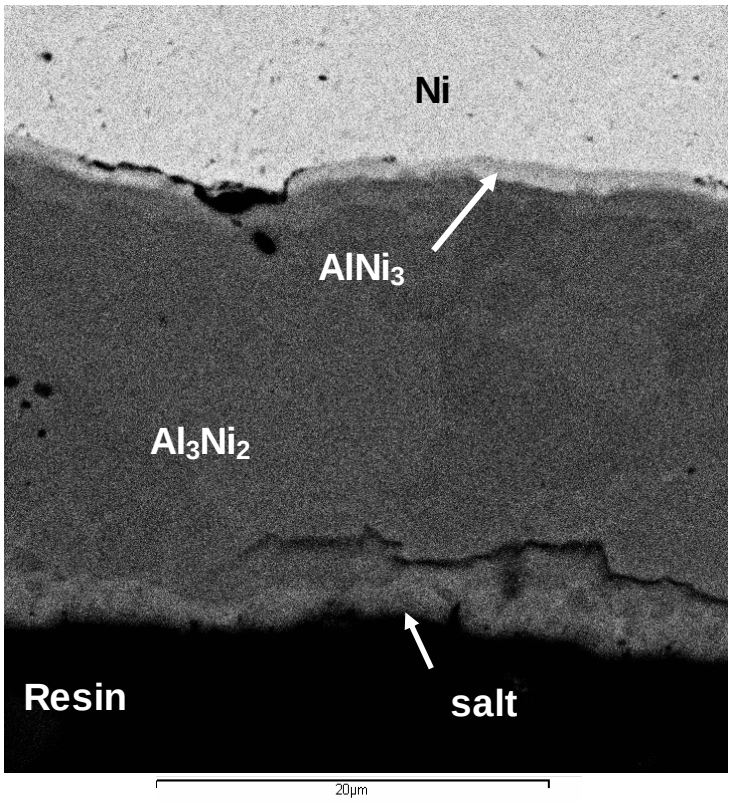

Figure 11b

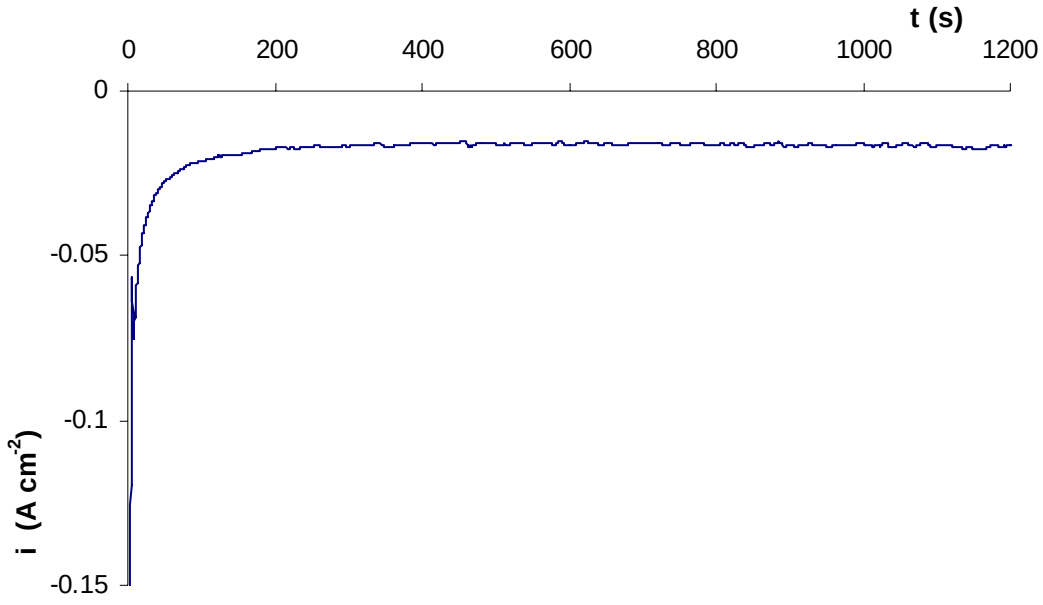

Figure 12

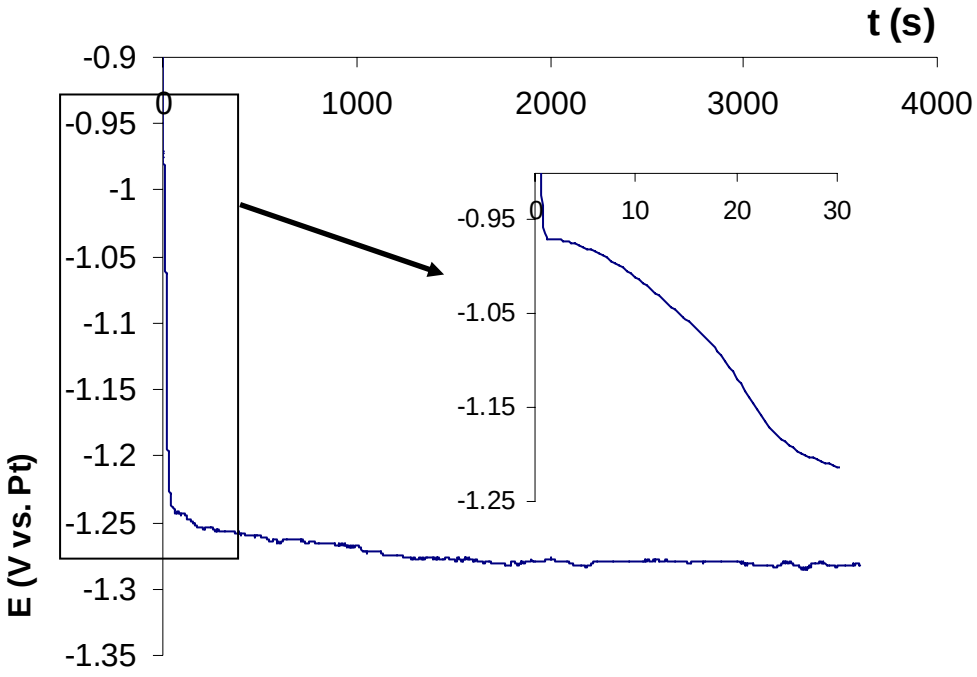
t (s)
-0.9
-0.95
-1
-1.05
-1.1
-1.15
-1.2
-1.25
-1.3
-1.35
E (V vs. Pt)
0
1000
2000
3000
4000
-0.95
-1.05
-1.15
-1.25
0
10
20
30

Figure 13

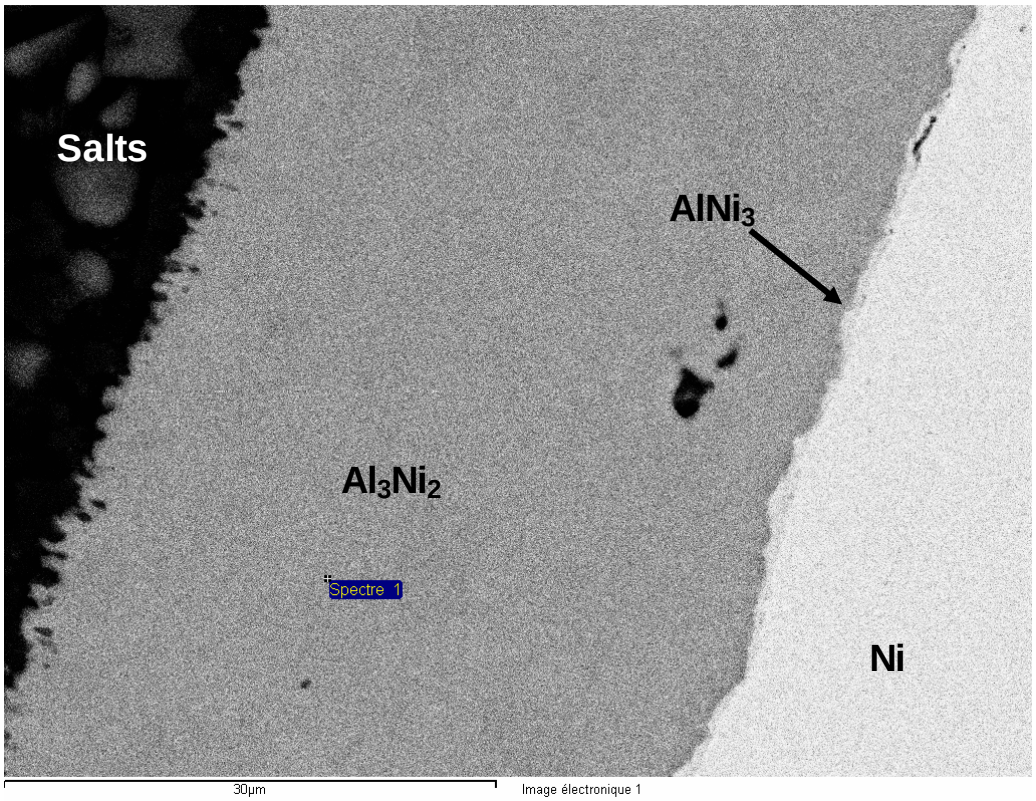

Figure 14a

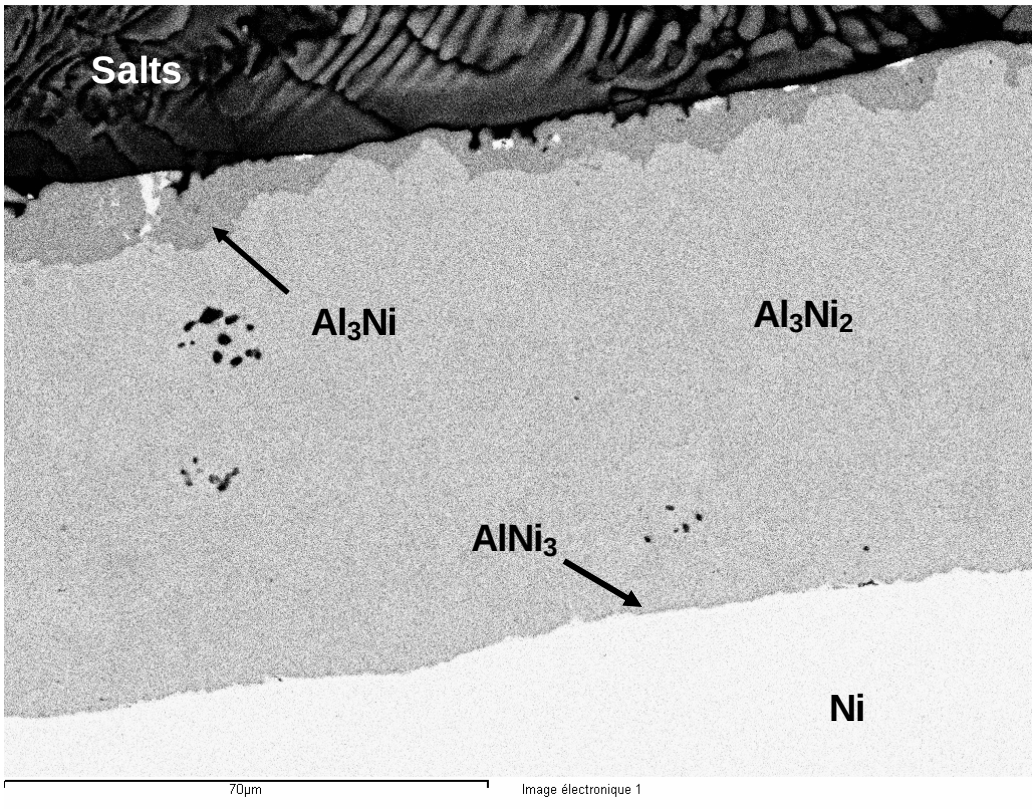

Figure 14b

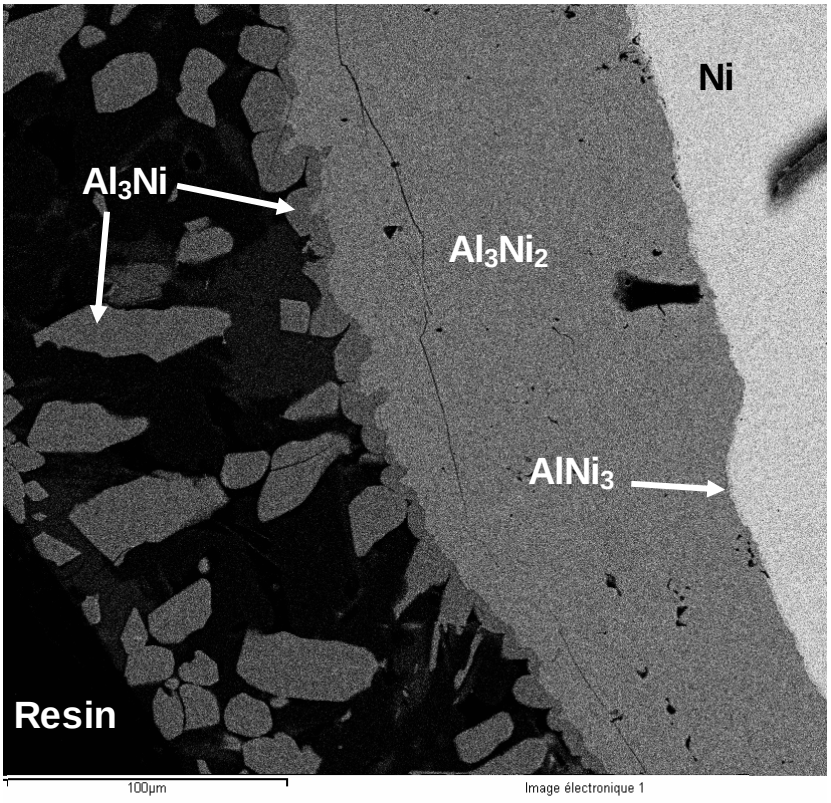

Figure 14c

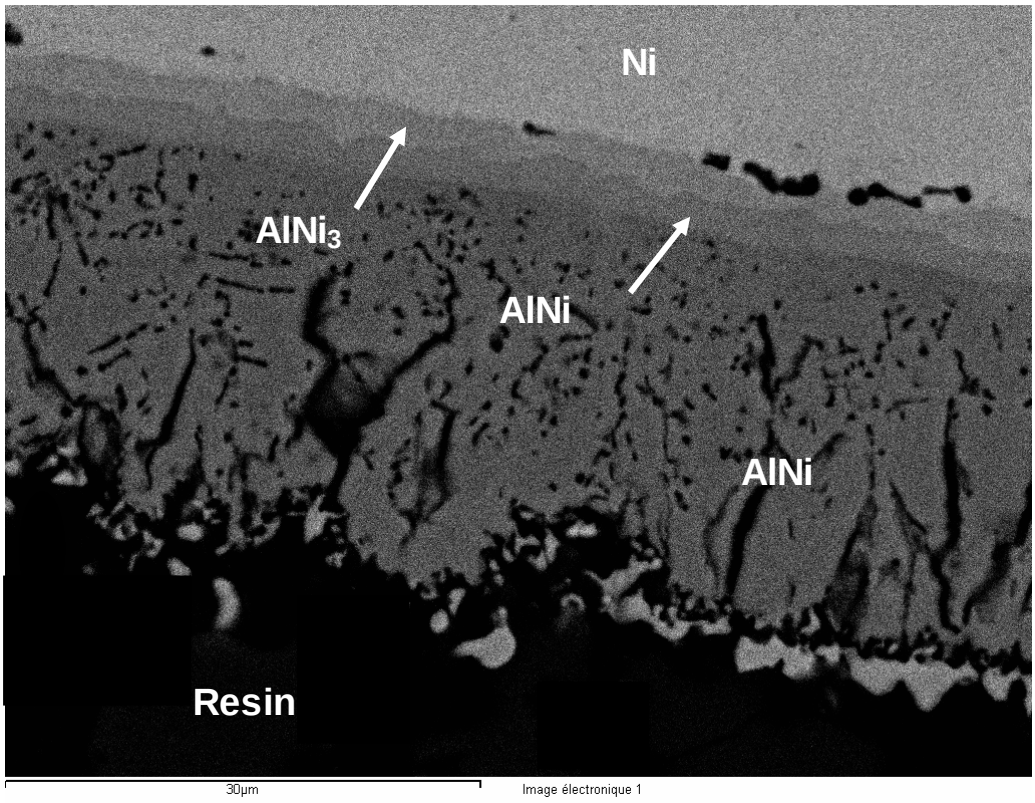

Figure 15a

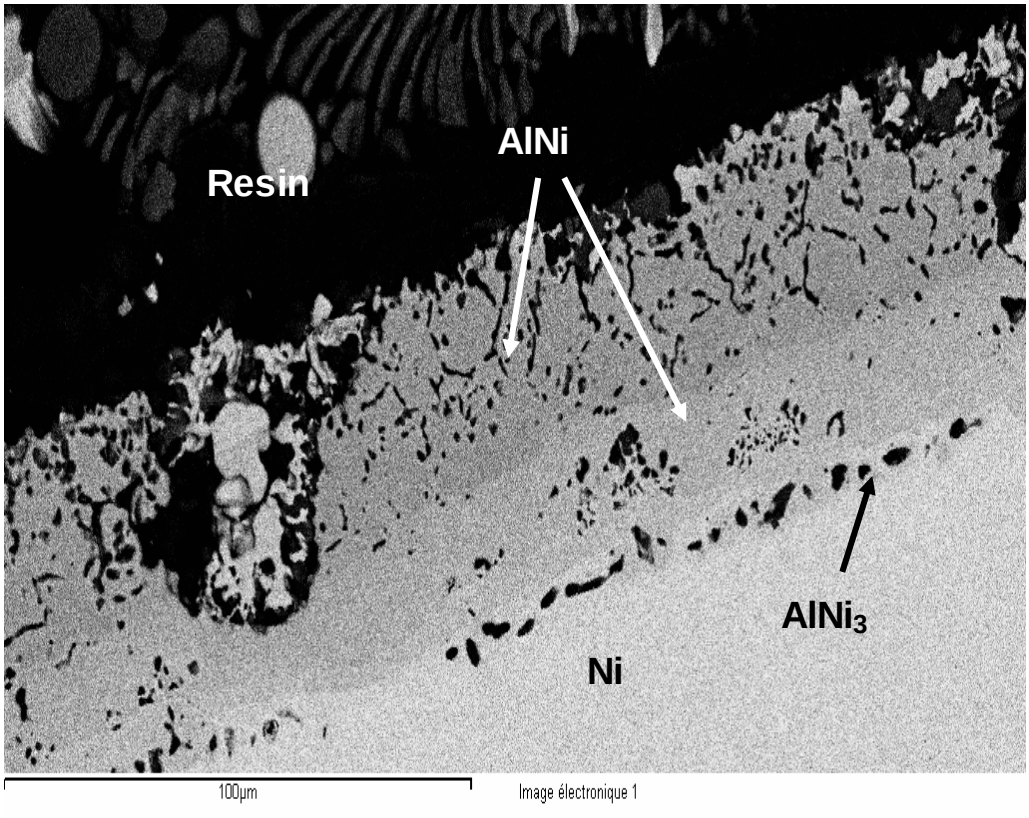

Figure 15b

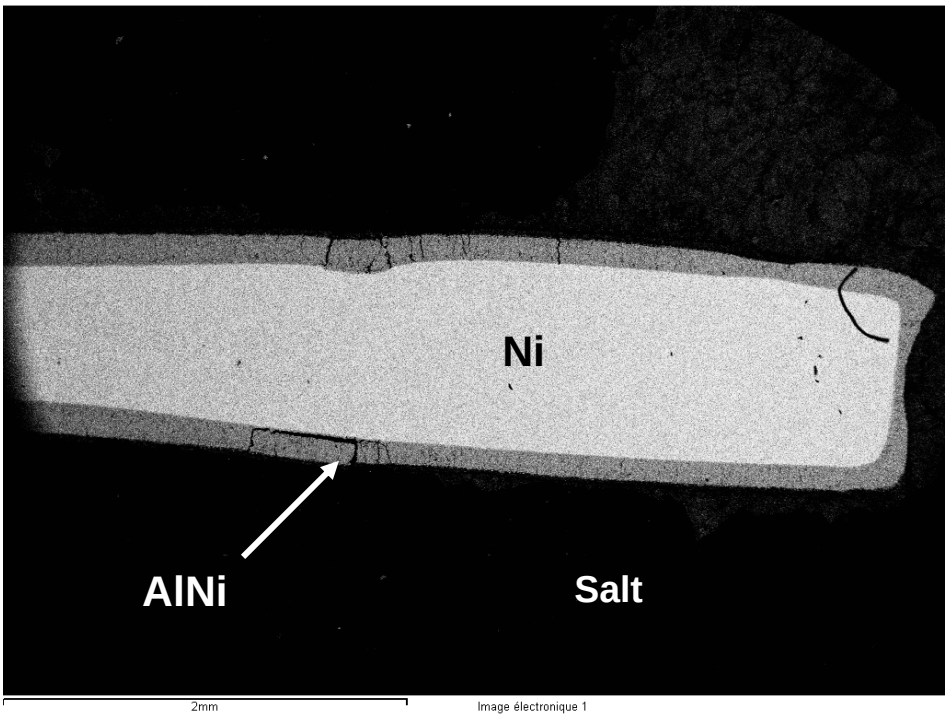

Figure 15c

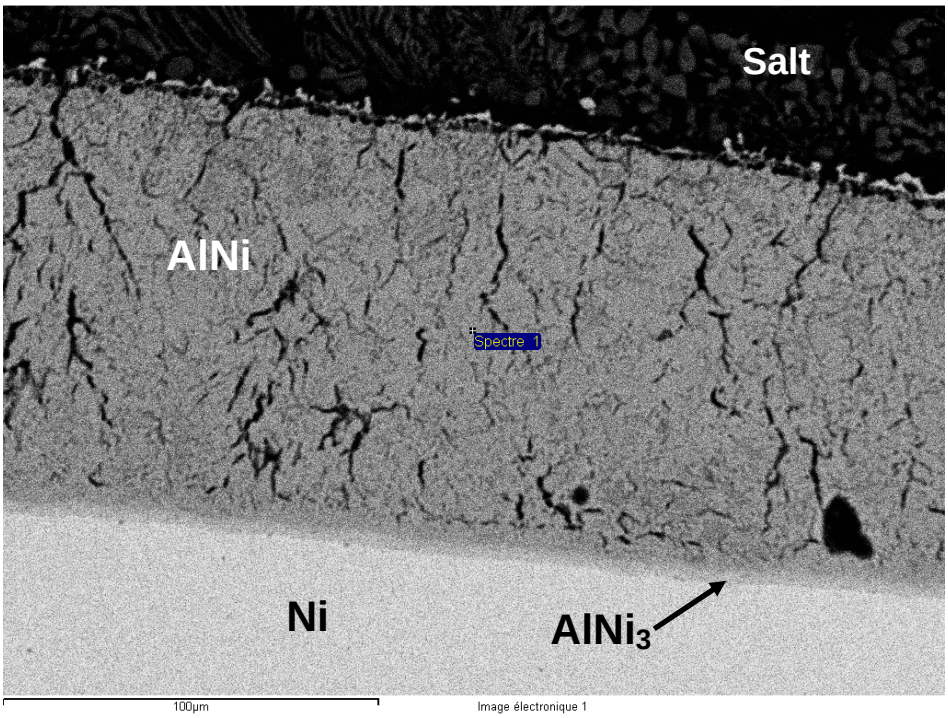

Figure 15d